nature communications

Article

https://doi.org/10.1038/s41467-025-56988-3

Rhizobacteria protective hydrogel to promote plant growth and adaption to acidic soil

Received: 16 June 2024

Accepted: 7 February 2025

Published online: 16 February 2025

Check for updates

Qirui Feng[1,2], Yu Luo[1,3], Mu Liang[1,2], Yingui Cao[4], LingShuang Wang[4], Can Liu[1,5], Xiaoyong Zhang[1,5], Lanyang Ren[1,5], Yongfeng Wang[6], Daojie Wang[6], Yantao Zhu[7], Yanfeng Zhang[7], Bo Xiao[4] & Nannan Li[1,2,7,8]

Endophytic plant growth promoting rhizobacteria (PGPRs) could replace chemical fertilizers in sustainable agriculture. Unfortunately, they are susceptible to harsh environmental conditions. Here, we proposed a polymeric hydrogel (PMH) consisting of carboxymethyl chitosan, sodium alginate, and calcium chloride for loading and protecting endophytic PGPR. This hydrogel can load endophytic PGPRs to not only boost its growth-promoting efficiency, but also help them adapt more effectively to environments. Using endophytic PGPR *Ensifer* C5 as model bacteria and *Brasscia napus* as host, we demonstrate that the PMH facilitate the colonization of endophytic PGPRs in the apical and lateral root primordia regions. Further analysis indicates that the PMH modulate suberin deposition of the endodermal cell layers and regulate the accumulation of auxin at the root tip. Meanwhile, PMH enhances the antioxidant capacity and disease resistance properties of plants by increasing the content of arachidonic acid metabolism intermediates in the plant. Importantly, the combination of PMH and endophytic PGPRs increases the yields of *B. napus* by approximately 30% in the field. Furthermore, PMH attenuates the loss of endophytic PGPR activity in the acidic environments. Overall, this microbial encapsulation strategy is a promising way to protect fragile endophytic microorganisms, providing attractive avenues in sustainable agriculture.

Globally, agricultural production has been one of the key industries supporting human survival and development. The global population is projected to reach 9.8 billion by 2050, with demand for food increasing by nearly 70 percent[1,2]. Agricultural production is also facing increasing challenges. Among them, accelerated urbanization, declining soil quality and environmental pollution caused by the excessive use of pesticides and fertilizers are becoming more prominent[3–5]. With the continuous development of global agricultural production and the improvement of people's awareness of food safety and environmental protection, there is an increasing demand for

[1]College of Resources and Environment, and Academy of Agricultural Sciences, Southwest University, Chongqing 400715, China. [2]Hanhong College, Academy of Agricultural Sciences, Southwest University, Chongqing 400715, China. [3]Yazhouwan National Laboratory, Sanya, Hainan 572025, China. [4]State Key Laboratory of Resource Insects, College of Sericulture, Textile, and Biomass Sciences, Southwest University, Chongqing 400715, China. [5]Key Laboratory of Low-carbon Green Agriculture in Southwestern China, Ministry of Agriculture and Rural Affairs, Interdisciplinary Research Center for Agriculture Green Development in Yangtze River Basin, Southwest University, Chongqing 400715, China. [6]College of Agriculture, State Key Laboratory of Crop Stress Adaptation and Improvement, Henan University, Kaifeng, Henan 475004, China. [7]Hybrid Rapeseed Research Center of Shanxi Province, Yangling, Shanxi 712100, China. [8]Research Center for Intelligent Computing Platforms, Zhejiang Lab, Hangzhou, Zhejiang 310012, China. e-mail: bxiao@swu.edu.cn; linannan2013@swu.edu.cn

efficient, environmentally friendly and sustainable agricultural production methods, and in order to achieve the United Nations sustainable development goals, it has become a pressing need to find new types of fertilizers to replace traditional chemical fertilizers[6,7].

Microbial fertilizers, as a new type of product that can replace chemical fertilizers, have attracted much attention because of their eco-friendliness and efficient soil amelioration capacity[8–10]. In particular, PGPRs are recognized as potentially beneficial microorganisms that are able to form a symbiotic relationship with plants to promote plant growth, enhance immunity, and improve the soil environment[11–14]. However, in practice, there are several challenges associated with direct soil application of PGPRs, such as low survival of microorganisms due to climate change and abiotic stressors (e.g., soil pH, temperature), which makes it difficult for microorganisms to be stabilized in the soil over time for growth-promoting effects[15–17], and be one of the major bottlenecks hindering the use of biofertilizers on a large scale.

Engineered materials have a wide range of applications in plants and have been shown to increase the efficiency of plant nutrient fixation to promote growth or to dynamically interact with the rhizosphere associated microbiome to improve plant health, while reducing conventional fertilizer application and increasing crop yields[18–20]. Notably, although nanomaterials can enable the attachment of various bioactives and microorganisms, thereby facilitating targeted delivery to specific cell types or organelles and are not limited by plant cell type, however, they are synthesized in a complex process, are potentially toxic to plant cells, and may face stability issues in the complex biological environments of the plant, which may reduce their overall delivery efficiency[21–23]. In contrast, biomaterials hold significant potential as microbial encapsulants due to their good biocompatibility and biodegradability[24]. Previously, microbial fertilizers made from PGPRs encapsulated in biomaterials have been reported to promote seed germination, protect microorganisms from desiccation stress, and also alleviate soil salinity[25,26].

Currently, some biofertilizer strains lack a competitive advantage over native soil microbial communities and are unable to colonize the plant root system for their growth-promoting effects[27]. We can use endogenous members of the core microbiome to reduce competition with the soil microbiome because these microorganisms will colonize the internal tissues of the plant and thus will be protected[28]. On the other hand, some encapsulants for biofertilizers face problems of not being cost-effective or taking a long time to prepare, or leading to a loss of microbial viability, not being able to be preserved for extended periods, and not being suitable for large-scale use[26,29]. Another important issue is the need for the strain to be suitable for colonization in the tissues of the respective plant species after it is encapsulated, as well as its ability to also exhibit the desired growth-promoting functions in the receiving environment, which is a major challenge for some

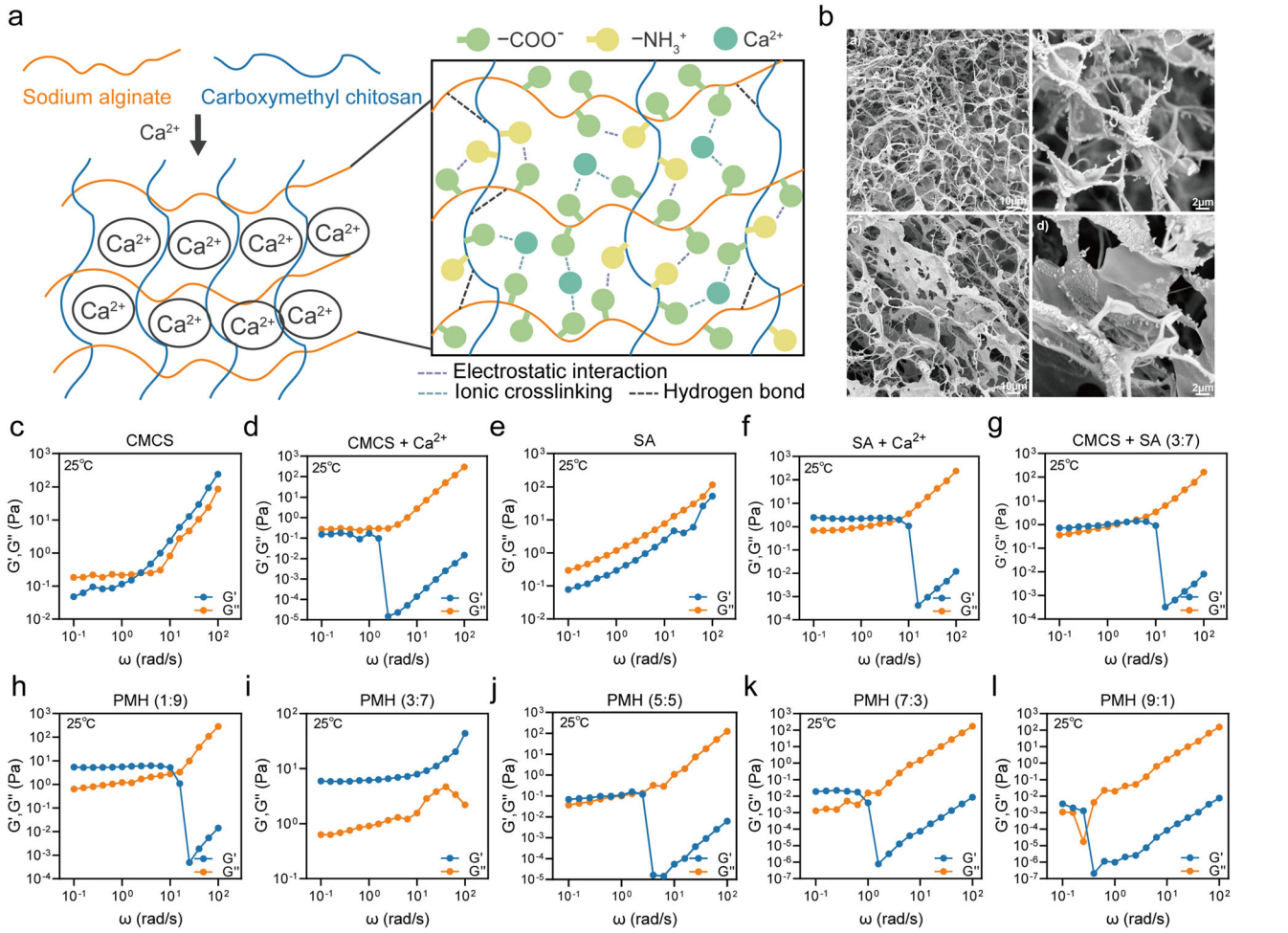

Fig. 1 | Structural characteristics of PMH (with Supplementary Fig. 1). a Schematic illustration of the preparation of CMCS/SA/$CaCl_2$ hydrogel. This figure was created with Adobe Illustrator (https://helpx.adobe.com/cn/support/illustrator.html). **b** Scanning electron microscope (SEM) images of the surface (**a**, **b**) and cross-section (**c**, **d**) of freeze-dried hydrogel. The micrographs (**a**, **c**) were taken with a magnification of 2,000 times, scale bar = 10 μm; micrographs (**b**) and (**d**) were taken at 10,000 times magnification, scale bar = 2 μm. **c**–**l** The elastic and viscous modulus curves of polymers containing some components of CMCS/SA/$CaCl_2$ hydrogels (**c**–**g**) and CMCS/SA/$CaCl_2$ PMH with different ratio of CMCS or SA (added $CaCl_2$) (**h**–**l**). All the measurements were repeated three times ($n = 3$).

biofertilizers[30]. Therefore, there is an urgent need to develop a novel, low-cost, and simple microbial encapsulant that preserves the activity of PGPRs over time and aids in the colonization of PGPRs, improves their growth-promoting efficiency and resists acidic environments.

In this work, we select endophytic PGPR *Ensifer* C5 as the basic strain for developing biofertilizers to improve the growth-promoting efficiency. Considering their susceptibility to harsh environmental conditions, carboxymethyl chitosan (CMCS), sodium alginate (SA), and calcium chloride ($CaCl_2$) are chosen for the formation of polymeric hydrogel (PMH) via interaction forces such as electrostatic attraction, ionic cross-linking, and hydrogen bonding. Utilizing plate, pot and field experiments, we determine that the PMH enhances the growth-promoting efficiency of PGPRs in multiple species and withstands acidic environments. A combination of fluorescence imaging and multi-omics analyses reveals the ability of PMH to facilitate the colonization of PGPRs within the plant root system, to alter the root diffusion barriers for optimizing the mineral-nutrient homeostasis and abiotic stress response of plants, to regulate phytohormone secretion, and to enhance plant metabolic activity and antioxidant activity in combination with PGPRs. The results contribute to improving the efficiency of agricultural production and reducing environmental pollution, which opens up the possibility of implementing biomaterials-supported agricultural practices in a sustainable manner.

Results

Synthesis and characterization of PMH

CMCS, SA, and $CaCl_2$ are cross-linked into chelates with three-dimensional spatial structures through electrostatic attraction, hydrogen bonding, and other interaction forces (Fig. 1a). The morphology of the lyophilized CMCS/SA/$CaCl_2$ PMH was characterized using scanning electron microscope (SEM) (Fig. 1b). The PMH showed a porous morphology on the surface and in the cross-section, and the connected small pores gave the PMH a large specific surface area, which helped to keep them moist and breathable, providing a suitable environment for bacterial propagation.

In the fourier transform infrared spectroscopy (FTIR) spectrum (Supplementary Fig. 1), the absorption peaks caused by the symmetric stretching vibrations of -COO^- shifted from 1416 cm^{-1} in SA to 1414 cm^{-1} in SA/Ca^{2+} and from 1414 cm^{-1} in CMCS to 1410 cm^{-1} in CMCS/Ca^{2+}, indicating that -COO^- is complexed with Ca^{2+} in SA or CMCS[31], and Ca^{2+} is binding with the -COO^- in a bidentate mode[32]; the absorption peak due to the symmetric stretching vibration of -COO^- shifted from 1416 cm^{-1} in SA to 1414 cm^{-1} in CMCS/SA, indicating that there is electrostatic attraction between -NH_3^+ in CMCS and -COO^- in SA[33]; the absorption peak corresponding to the O-H stretching vibration at 3500-3200 cm^{-1} shifts from 3339 cm^{-1} in CMCS and 3319 cm^{-1} in SA to 3269 cm^{-1} in PMH, suggesting that hydrogen bonding is involved in the formation of PMH[34].

In the rheological frequency scanning curves, the combination of CMCS and SA increased G′ compared to CMCS, SA individually, indicating electrostatic attraction between -NH_3^+ of CMCS and -COO^- of SA (Fig. 1c, e, g); the addition of Ca^{2+} to CMCS and SA, respectively, resulted in a more stable structure, suggesting that Ca^{2+} underwent ionic cross-linking with the -COO^- of CMCS and SA (Fig. 1c–f) and significantly improved the stability of the PMH (3:7) structure (Fig. 1g, i). Appropriate mechanical properties are important for microbial encapsulants to maintain the integrity of the PGPRs when the biofertilizer is deformed by external forces. In the frequency scanning range of 0.1–100 Hz, the energy storage modulus G′ was always higher than the elastic modulus G″ for all hydrogels at lower frequencies. When the frequency gradually increased, the G′ of PMH (1:9), PMH (5:5), PMH (7:3), and PMH (9:1) started to decrease, and G″ started to be higher than G′, indicating that the structure was disrupted; however, the energy storage modulus of the PMH (3:7) hydrogel was always higher than the loss modulus (Fig. 1h–l), which indicated that the PMH (3:7) was structurally stable and elastic, and is an ideal material for microbial encapsulants[35].

PMH demonstrates the ability to serve as encapsulating agents for biofertilizers

After encapsulation of PGPRs with SA, it was mixed well with CMCS and $CaCl_2$ to make biofertilizer (Fig. 2a). SEM photographs showed that C5 was encapsulated in the spatial mesh structure of PMH (Fig. 2b). TEM images further demonstrated the successful encapsulation of PMH on C5 (Fig. 2c). OD_{600} was determined by encapsulating C5 with CMCS, SA, a mixture of CMCS and SA (with added Ca^{2+}), and PVP and MC, which are commonly used to encapsulate microorganisms, and it was found that encapsulation of C5 with PMH (3:7) did not affect the survival of C5, and yet there was a significant difference in the reproduction rate of C5 encapsulated with PMH (3:7) and other encapsulants (Fig. 2d). This demonstrated that PMH (3:7) had the best encapsulation performance and favored the survival and multiplication of C5. Moreover, after the standard curve was measured with Alamar Blue (Supplementary Fig. 2), the bacterial activity of C5 was determined in the first, third and fifth weeks, and it was revealed that PMH (3:7) favored the long-term storage of C5, which is more conducive to agricultural practices (Fig. 2e). For determining the efficacy of the CMCS/SA/Ca^{2+} polymer matrix in releasing PGPRs, we monitored the release process. The results showed that the PMH was able to release PGPRs rapidly, which further supported the efficacy of the system (Fig. 2f)[36].

PMH improves the growth-promoting efficiency of PGPRs in multiple plant species

To reveal the potential positive effects of PMH-encapsulated endophytic PGPRs on plant growth, we used C5-loaded PMH (3:7) as a biofertilizer applied directly to the soil and set up to treat the plants with a combination of sterile water (CK), PMH, and C5. C5 is a endophytic PGPR isolated in our laboratory. C5 improves *B. napus* growth under low phosphorus conditions (unpublished). After 21 days of growth of *B. napus* (*Zhongshuang 11*) seedlings, C5 was more efficient in promoting the growth of *B. napus* seedlings in the C5-PMH group compared with C5 treatment (Fig. 3a, b). The shoot fresh weight and dry weight, root fresh weight and dry weight increased to 1.41, 1.47, 1.58, and 1.49 times, respectively (Fig. 3c, d). Leaf area, stem diameter, root length and net photosynthetic rate correspondingly increased to 1.60, 1.19, 1.29 and 1.27 times (Fig. 3e–h), while lateral root length, number of lateral roots and root density also increased significantly (Supplementary Fig. 3d–f). The expression of functional genes in *B. napus* roots associated with C5, such as *PHT* and *PHR* family genes[37,38], showed a similar pattern of enhancement (Supplementary Fig. 3g). It is worth noting that the physiological indices of the plants in the PMH group were not significantly different from those of the CK group ($p > 0.05$), which excluded the effect of the PMH themselves on the plants. In the field experiment, similar effects were observed in dry weight, fresh weight, stem diameter, and shoot length of *B. napus* at the seedling stage after the application of biofertilizer (C5-PMH) compared with the C5 group (Supplementary Fig. 4) and the number of pods and yield of the final plants were increased by 30.74% and 28.01%, respectively (Fig. 3k–m). In addition, a similar pattern of increased C5-promoting efficiency by PMH was observed in the yields of *B. napus* (*Zhongshuang 11*), *Pakchoi* (*Jinzhi 30*), and in *Arabidopsis thaliana* (Col-0) yields in the sterile environments we tested (Supplementary Figs. 5, 6). These results suggest that PMH-mediated enhancement of PGPRs promotion efficiency remains applicable in different species and can be utilized in practical production.

https://doi.org/10.1038/s41467-025-56988-3

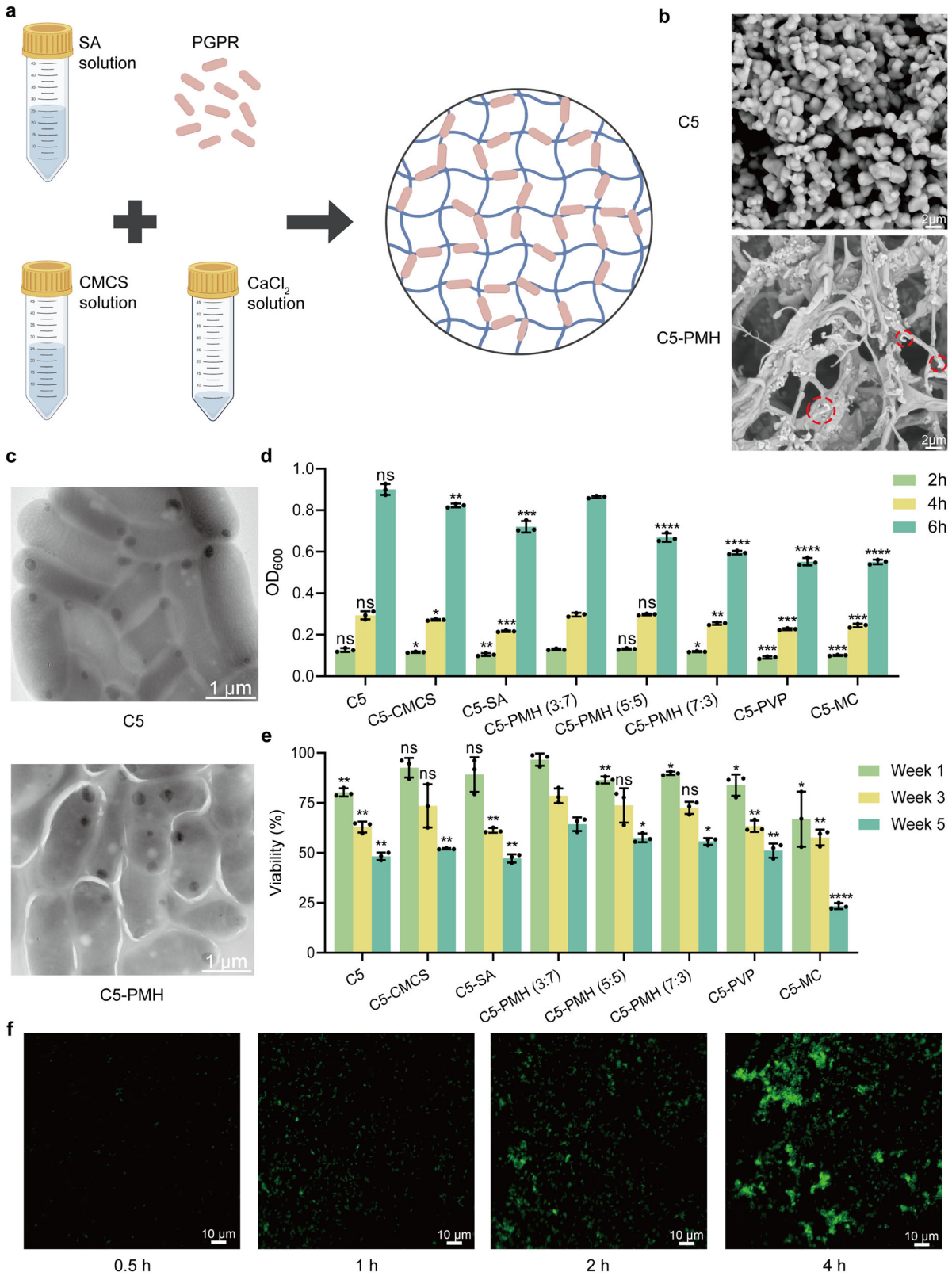

PMH facilitates the colonization of endophytic PGPRs inside the root system to mediate the regulation of endodermal root diffusion barriers and plant hormones

To investigate whether PMH is beneficial in assisting the colonization of PGPRs in plant roots, we modified C5 (GFP-C5) with green fluorescent protein (GFP) to visualize the distribution of the bacteria in plant roots. In Fig. 4, we report fluorescence images of *B. napus* root systems treated with GFP-C5 or GFP-C5-loaded PMH. Fluorescence imaging of roots showed that C5-loaded PMH promoted C5 colonization in primary and lateral roots as well as lateral root primordia at different levels of development, and resulted in a significant accumulation of C5 in root cross sections as well (Fig. 4a, c, e, g). The relative fluorescence intensity of C5-loaded PMH-treated plants was significantly higher than that of C5-treated plants (Fig. 4b, d, f, h), further

Fig. 2 | Encapsulation and feasibility of biofertilizers. a Schematic diagram of encapsulation for the preservation and delivery of PGPRs in biofertilizers. Some of the elements of this figure are by figdraw.com. Created in BioRender. QR, F. (2025) https://BioRender.com/i02e296. **b** Scanning electron microscope (SEM) micrograph depicting the attachment of C5 within the three-dimensional lattice structure of the encapsulant (Some C5 particles are highlighted within the red circle). Both micrographs were taken at 10,000x magnification, scale bar = 2 μm. **c** Representative TEM images of C5 and C5-loaded PMH (C5-PMH), scale bar = 1 μm. **d** OD_{600} measurements of C5 liquid cultures preserved in CMCS, SA, CMCS and SA mixtures with added $CaCl_2$, and other encapsulation materials such as PVP and MC showed significant differences between 2 and 6 h. **e** The bacterial activity of C5 encapsulated with the different encapsulants mentioned above was determined at weeks 1, 3 and 5. "*" indicates comparison with the C5-PMH (3:7) group in each group. **f** Representative images of GFP-C5 release by biofertilizers, scale bar = 10 μm. Each experiment was repeated three times independently with similar results in (**b**, **c**–**f**). The error bars in (**d**, **e**) are the SD of 3 biological replicates ($n = 3$). Statistically significant differences between the means were analyzed with two-tailed Student's *t*-test (*$p < 0.05$; **$p < 0.01$; ***$p < 0.001$; ****$p < 0.0001$) in (**d**, **e**).

demonstrating that PMH can enhance the colonization rate of PGPRs in the plant root system to promote plant growth.

To illustrate the effect of PMH-encapsulated PGPRs on the deposition of suberin in the endodermis, we performed plate experiments and stained whole roots of seedlings using Fluorol Yellow 088 and aniline blue. The results showed that the primary root length of *gpat5* became shorter under the same treatments (Fig. 5a, b). Furthermore, in both WT and *gpat5*, the root zone with continuous activation of CK, C5 and C5-PMH groups were sequentially reduced and sequentially expanded the root zone following a patchy pattern (Fig. 5c, f). Thus, C5-loaded PMHcould better optimize plant mineral nutrient homeostasis and abiotic stress responses by regulating the establishment of endodermal diffusion barriers in the root system[39].

We used *DR5::GFP* transgenic plants to visualize growth hormone distribution in the root system[40]. Root fluorescence imaging showed that C5-loaded PMH (C5-PMH) promoted the production and accumulation of growth hormone in root tip and lateral root primordia (Fig. 5d, e).The relative fluorescence intensity of CK, C5, and C5-PMH group plants was significantly increased and there was no significant difference between CK and PMH groups (Fig. 5g), demonstrating that PMH can assist PGPRs to promote root growth by regulating the growth hormone content of root tip and lateral root primordia to promote root growth.

PMH contributes to enrichment of endophytic PGPRs abundance in roots and enhancement of antioxidant activity and metabolism in plants by binding PGPRs

To determine whether PMH is beneficial to the enrichment of endophytic PGPRs, or whether they lead to changes in the entire microbial community, we performed 16S rRNA sequencing of rhizosphere soils (S) and roots (R) from each treatment. Differences in β-diversity were observed by principal coordinate analysis (PCoA, based on Bray-Curtis distance), with large differences in species types and relative abundance between groups, suggesting that the individual treatments were effective (Fig. 6a, b). Colony composition analysis at the genus level showed that *Ensifer* abundance was more abundant in the roots of the C5 and C5-PMH groups and was significantly higher in the roots of the C5-PMH group than in the C5 group, whereas *Ensifer* abundance was less abundant in the roots of the CK and PMH groups and there was no significant difference between them. *Ensifer* abundance in the rhizosphere soils of all treatments was rare (Fig. 6c). At the species level, *g_Ensifer* was found to be the most prevalent and significantly different between the C5 and C5-PMH groups (Fig. 6d). Further analysis at the ASV level showed that C5 content in roots was sequentially increased in the CK, C5, and C5-PMH groups, and there was no significant difference between the CK and PMH groups. (Fig. 6e). These results suggest that PMH contributes to enriching the abundance of PGPRs in the roots to improve the growth-promoting efficiency of PGPRs.

To further investigate the mechanism of action of C5-loaded PMH (C5-PMH), we performed LC-MS untargeted metabolomics analysis on root samples. Principal component analysis (PCA) revealed that wrapping C5 with PMH significantly altered the metabolites of *B. napus* roots (Fig. 6f). The annotated biological processes of metabolites were summarized by KEGG enrichment analysis, the "arachidonic acid metabolism" pathway and the "ascorbate and aldarate metabolism" pathway were significantly enriched in the C5-PMH group (Fig. 6g). Arachidonic acid is an ω-6 polyunsaturated fatty acid that acts as a signaling molecule in plants, triggering fatty acid-mediated defense responses and triggering a general stress signaling network, thereby improving antioxidant and disease resistance properties of plants[41,42]. The "ascorbate and aldarate metabolism" pathway is recognized as an antioxidant defense-related pathway that protects cells from oxidative stress[43,44]. The variable importance in projection (VIP) score was utilized to determine the separation potential of the metabolites. According to our predefined criteria ($p < 0.05$, VIP > 1 and |fold change| > 1.2), 16 metabolites were demonstrated to be differentially expressed after wrapping C5 with PMH (Fig. 6h). The intermediates 12(R)-HPETE and 8,9-Epoxyeicosatrienoic acid of the "arachidonic acid metabolism" pathway were considerably increased, which favored the upward movement of arachidonic acid content. Interestingly, Lipoamide was significantly up-regulated in expression, while Pyruvic acid was significantly down-regulated. A plausible explanation for this may be that Lipoamide is a key cofactor in the pyruvate dehydrogenase complex (PDC) and the α-ketoglutarate dehydrogenase complex that catalyzes acyl transfer. All of these complexes act in cellular metabolism, especially linking glycolysis and the tricarboxylic acid cycle. And they are responsible for the conversion of pyruvic acid produced in the metabolism of sugars into acetyl CoA, which in turn is involved in the production of energy[45–47]. Furthermore, the activity of dihydrolipoic amide dehydrogenase, one of the components of the above complex, stimulates photosynthetic carbon assimilation and plant growth by boosting the efficiency of photorespiration[48]. These results suggest that C5-loaded PMH enhances plant antioxidant activity and participate in energy production and plant photorespiration.

PMH mitigates soil acidity for endophytic PGPRs, thereby enhancing the adaptabiligy of crops to acidic soil

To investigate whether PMH has the potential to contribute to the resistance of PGPRs to abiotic stresses, such as acidic soil, we tested the rheological properties of PMH with different ratios of components and the effect of PMH on C5 in an acidic environment (pH = 5.5). We found that PMH (3:7) remained structurally stable and elastic in acidic environment (pH = 5.5), making it an ideal material for microbial encapsulants (Supplementary Fig. 7a–e). By making a growth curve in LB medium at pH = 5.5 (Fig. 7a), we found that the C5-PMH group showed a significant increase in OD_{600} compared to the C5 group ($p < 0.05$), and the results were similar on the solid plate (Supplementary Fig. 7f). Plate experiments further verified that PMH can resist acidic environment for PGPRs (Fig. 7b–h). Shoot fresh weight, root fresh weight, and lateral root length were similar to the results in the neutral environment, and were increased to 1.40, 1.51, and 1.35 times in the C5-PMH group compared with the C5 group, respectively (Fig. 7c–e). It is noteworthy that due to the inhibition of C5 by the acidic environment, there was no significant difference ($p > 0.05$) between the C5 and CK groups in terms of lateral root number and lateral root density, whereas the promotion efficiency of the C5-PMH group was significantly increased to 1.32, 1.34 times, respectively, when

https://doi.org/10.1038/s41467-025-56988-3

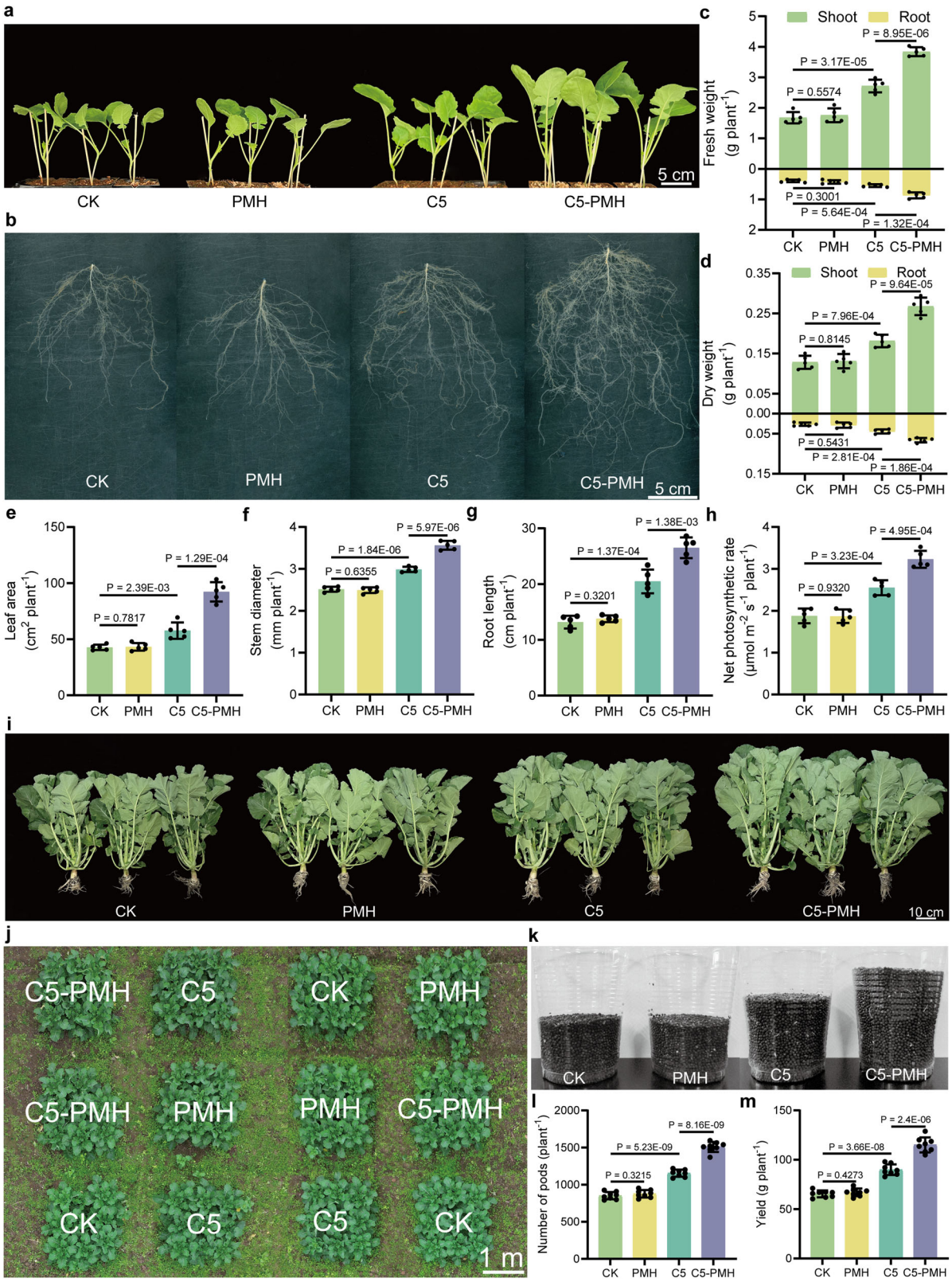

compared with that of the C5 group (Fig. 7f, g). By measuring the number of lateral roots of *B. napus* seedlings in each treatment per day, we found that the difference in the number of lateral roots between the C5 and C5-PMH groups could be observed starting at 4 days after germination, and that there was no significant difference ($p > 0.05$) between the CK, PMH, and C5 groups (Fig. 7h). These growth-promoting effects result from the fact that PMH mitigates the loss of vigor of PGPRs and promotes the colonization of endogenous PGPRs within the root system, thereby mediating the regulation of the root endodermal diffusion barrier in acidic environments (Supplementary Figs. 8, 9), which provides a promising solution to the problem of crop yield limitation by acidic soils.

Fig. 3 | PMH significantly enhances the growth-promoting efficiency of PGPRs to promote growth in different plant species (with Supplementary Figs. 3–6). **a**, **b** Representative images of *Brassica napus* (*Zhongshuang 11*) seedlings grown in potted soil (unsterilized) treated with the control group (CK), polymeric hydrogel (PMH), plant growth-promoting rhizobacteria C5, and C5-loaded PMH (C5-PMH), scale bar = 5 cm. **c**, **d** Quantification of fresh weight (**c**) and dry weight (**d**) of shoot and root. **e**–**h** Quantification of leaf area (**e**) stem diameter (**f**), root length (**g**) and net photosynthetic rate (**h**). **i** Representative images of *Zhongshuang 11* seedlings grown in field soil treated with the control group (CK), polymeric hydrogel (PMH), plant growth-promoting rhizobacteria C5, and C5-loaded PMH (C5-PMH), scale bar = 10 cm. **j** Distribution of individual treatment groups of *Zhongshuang 11* cultivated in Chongqing Academy of Agricultural Sciences (106°21′78″E, 29°27′57″N). **k** Representative images of yields for each treatment in the field experiment, scale bar = 5 cm. **l**, **m** Quantification of number of pods (**l**) and yield (**m**). The error bars in (**c**–**h**) are the SD of 5 plants per biological repeat ($n = 5$); those in (**l**, **m**) are the SD of 8 plants per biological repeat ($n = 8$). Statistically significant differences between the means were analyzed with two-tailed Student's *t*-test in (**c**–**h**, **l**–**m**).

Discussion

In this study, we developed a biomaterial-based method for encapsulating, preserving, and delivering PGPRs. The inexpensive and easy-to-prepare PMH can maintain the activity of PGPRs over time, facilitate the colonization of endogenous PGPRs in the stele of the plant root system, influence phytohormone secretion and suberin accumulation, enhance plant antioxidant activity and metabolic capacity, and thus promote plant growth and protect PGPRs from the acidic environment (Fig. 8). As biodegradable biomaterials, they are not toxic to the plants and the environment, indicating their potential prospects for extensive application in agriculture.

CMCS and SA are natural polysaccharides, inexpensive, biocompatible, biodegradable, and simply mixed in the preparation of biofertilizers, whereas many other materials do not satisfy all these advantages at the same time, which is very important for the large-scale use of microbial fertilizers[22,23,26,29,49]. We compared the rheological properties of CMCS:SA = 1:9, 3:7, 5:5, 7:3, and 9:1, and screened PMH (3:7) as the optimal ratio, which is structurally stable and resilient, and is a potential microbial encapsulant[35]. Encapsulants are crucial for the long-term preservation of the activity of PGPRs, and we compared them with the common commercially available PGPR encapsulants PVP and MC, and PMH (3:7) still performed well and efficiently released PGPRs[26,36].

We selected endophytic PGPRs isolated from within the root system of*B. napus*, which reduces competition between PGPRs and the soil microbiota compared to selecting biofertilizers with nonendophytic bacteria because these microorganisms colonize the internal tissues of the plant and are thus protected for consistent and stable growth promotion[27,28]. However, endophytic PGPRs still require protection against abiotic environmental stresses and need protection to help them colonize efficiently in the interior[15–17]. Surprisingly, we found that PMH was able to promote the colonization of PGPRs in the stele of the plant root system, thus acting directly to improve the growth-promoting efficiency. In the fields of biology, food and medicine, it has been shown that biocompatible microbial encapsulants can protect and release probiotics and promote their colonization at the target site, thus creating a dose effect and amplifying the effects of probiotics, which coincides with the results of this study[50–53].

Physicochemical characterization of strain C5 showed several significant plant growth-promoting parameters such as aiding Indole-3-Acetic Acid secretion, promoting lateral root growth, and altering the root diffusion barriers[39,54]. Visualization results of *DR5::GFP* transgenic plants and whole-root suberin staining of *A. thaliana* seedlings proved the dosage effect of PMH on C5. PMH assisted C5 in regulating the accumulation of auxin at the root tip and thus promoted root growth[55]. PMH increased the impact of C5 on the deposition of suberin in the endodermis of the root, resulting in fewer contiguous zones and more patchy zones of suberin in the root, which supported the homeostasis of phytomineral nutrients[39,56]. In the metabolome data, indoles were increased to 1.1–1.2 times in the roots of the C5-PMH group compared to the C5 group ($p < 0.05$), probably due to the fact that the same mass of samples was analyzed and the biomass of the roots of the C5-PMH group was about 1.5 times of the biomass of the roots of the C5 group, and thus, the amount of indoles in the roots of a single root of the C5-PMH group was still significantly higher than that of the C5 group. In addition, this method improves the metabolic activity and antioxidant capacity of the plant[56].

Acidic soils dramatically limit crop yields globally, since approximately 50 percent of all arable land in the world is acidic[57]. We tested the rheological properties of PMH in acidic environments, and similar to neutral environments, PMH (3:7) remains the most desirable microbial encapsulant material. In the biomedical field, probiotics encapsulated with the active ingredient alginate, when administered orally, can reduce the loss of viability of probiotics as they pass through the acidic environment of the stomach because alginate shrinks and produces a barrier-like structure to block the acid[58,59]. Excitingly, we also found that PMH can contribute to the resistance of PGPRs to abiotic stresses, such as acidic soil. Additionally, similar to neutral environments, in acidic environments, we discovered that PMH also promoted the colonization of PGPRs inside the root system and influenced the deposition of suberin in the roots, which resulted in a better optimization of plant mineral nutrient homeostasis and abiotic stress responses. These results offer a promising solution for improving crop yields in acidic soils.

Our study shows that for sustainable applications of agricultural improvement, the utilization of functional engineered material platforms for plant growth is reliable and not limited to delivery and enrichment of PGPRs, e.g., to potentiate plant disease resistance, we can exploit the material itself or as a carrier for delivery of nutrients or drugs to target specific plant pathogens[60,61]. Our research informs the design of biofertilizers or biopesticides involving the plant root system, but the molecular mechanisms involved in the plant response and the complex components (e.g., organic matter) of the soil environment need to be explored in further depth.

Methods

Chemical reagents

All reagents were used directly as received without further purification. Sodium Alginate (SA), Methylcellulose (MC) were purchased from Aladdin. Carboxymethyl Chitosan (CMCS), Polyvinylpyrrolidone (PVP) were purchased from McLean. Calcium Chloride ($CaCl_2$) was purchased from ChronChemicals. Alamar Blue was purchased from Yeasen. L-(+)-Lactic acid was purchased from Sangon Biotech. Fluorol Yellow 088 and aniline blue were purchased from Sigma-Aldrich. Sodium Hypochlorite was purchased from Energy Chemical.

Synthesis of PMH

SA powder was dissolved in 0.15 mol/L NaCl solution to achieve a concentration of 1.4% (wt/vol); CMCS powder was dissolved in an aqueous solution to achieve a concentration of 0.6% (wt/vol); and a $CaCl_2$ chelating solution with a concentration of 0.07 mol/L was equipped. The sterilized SA solution and CMCS solution were mixed at a volume ratio of 1:1 to a final concentration of 7 g/L and 3 g/L, respectively, and mixed well, then a sterile $CaCl_2$ solution with 10% of the above polymer volume was added and mixed well to obtain CMCS/SA/$CaCl_2$ PMH. PVP and MC powders were dissolved in water, respectively, to obtain the biopolymer solution with a concentration equal to the above PMH and sterilized.

https://doi.org/10.1038/s41467-025-56988-3

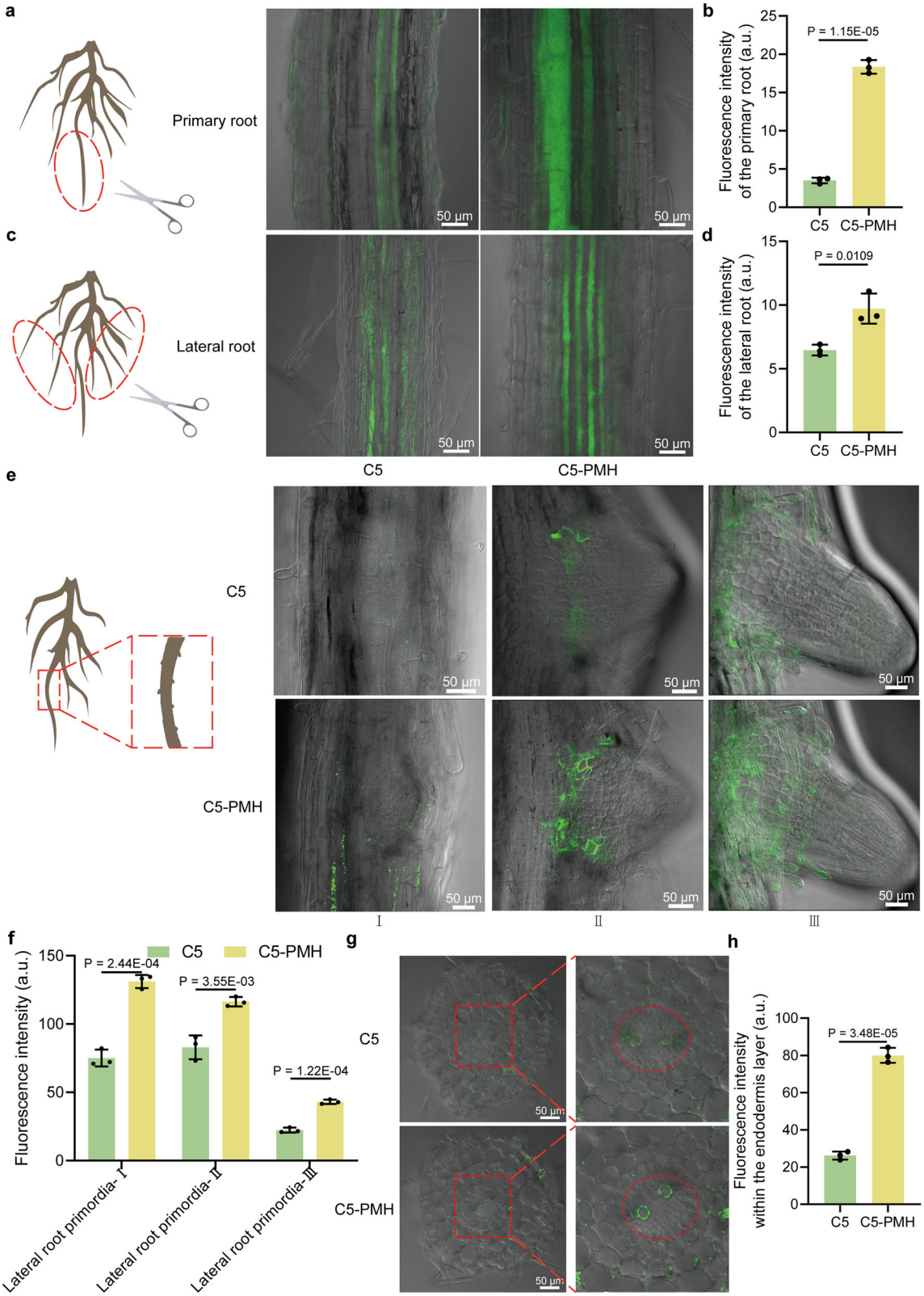

Fig. 4 | PMH facilitates the colonization of PGPRs within the plant root system. **a**–**g** Fluorescence images show the amount of C5 colonized in the primary roots (**a**), the lateral roots (**c**) the different stages of lateral root primordia (**e**), and the lateral root transverse sections (**g**) of *Brassica napus* treated with GFP-C5 or GFP-C5-loaded PMH. **b**, **d**, **f** and **h** Relative fluorescence intensity of the primary roots (**b**) the lateral roots (**d**) the different stages of lateral root primordia (**f**), and the lateral root transverse sections (**h**) which suggest that PMH assists PGPRs enrichment inside the plant root system. **a**–**e** were created by figdraw.com. The error bars in (**b**–**h**) are the SD of 3 plants per biological repeat ($n = 3$). Statistically significant differences between the means were analyzed with two-tailed Student's *t*-test in (**b**–**h**).

https://doi.org/10.1038/s41467-025-56988-3

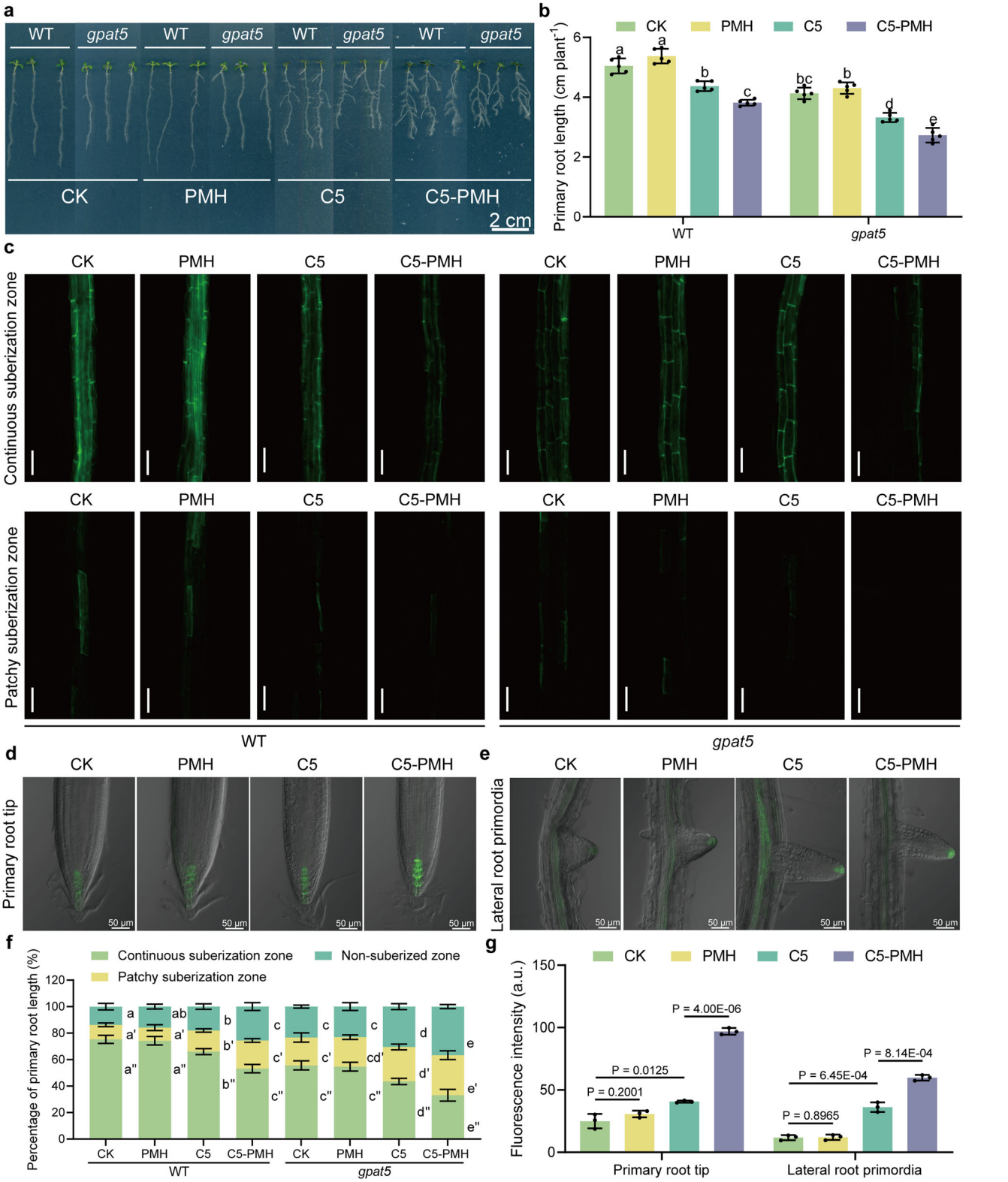

Characterization of PMH

The FTIR spectrum were recorded by a BRUKER TENSOR 27 (Bruker, Germany) with the wavenumber ranging from 4000 – 400 cm^{-1}. Each sample was prepared using the potassium bromide method[62]. The surface and cross-section of the lyophilized specimens was sprayed by gold and the morphologies of the samples were examined by a Phenom Pro SEM (Phenom World, the Netherlands). The sterile CMCS solution and SA solution as described above were mixed in total ratios of CMCS to SA of 1:9, 3:7, 5:5, 7:3, and 9:1, respectively. Subsequently, a sterile $CaCl_2$ solution, constituting 10% of the polymer volume, was added to the mixture and uniformly blended to obtain a hydrogel. The hydrogel was then applied to cover the testing probe model PP25. The rheological properties of the CMCS/SA/$CaCl_2$ hydrogels were

https://doi.org/10.1038/s41467-025-56988-3

Fig. 5 | PMH assists PGPRs to mediate the regulation of endodermal root diffusion barriers and plant hormones. a Representative images of *A. thaliana* (Col-0 and *gpat5*) seedlings grown in culture medium treated with the control group (CK), polymeric hydrogel (PMH), plant growth-promoting rhizobacteria C5, and C5-loaded PMH (C5-PMH), scale bar = 2 cm. **b** Quantification of primary root length. **c** Fluorescence images show suberin in similar parts of the root of *A. thaliana* (Col-0 and *gpat5*) treated with Fluorol Yellow 088 and aniline blue, scale bar = 50 μm. **d**, **e** Fluorescence images show auxin expression in primary root tip (**d**) and lateral root primordia (**e**) of *A. thaliana* (*DR5::GFP*) treated with polymeric hydrogel (PMH), plant growth-promoting rhizobacteria C5, and C5-loaded PMH (C5-PMH), scale bar = 50 μm. **f** Quantification of suberin deposition in three different regions: non-suberized; patchy; and continuous. **g** Relative fluorescence intensity of the primary root tip and lateral root primordia. Each experiment was repeated three times independently with similar results in **a** and **c**–**e**. The error bars in (**b**) are the SD of 5 plants per biological repeat ($n = 5$); those in (**f**) are the SD of 6 plants per biological repeat ($n = 6$) and those in (**g**) are the SD of 3 plants per biological repeat ($n = 3$). Different letters indicate statistically significant differences among genotypes (**b**, **f**) based on one-way ANOVA and Tukey's HSD test analysis ($p < 0.05$). Statistically significant differences between the means were analyzed with two-tailed Student's *t*-test in (**g**).

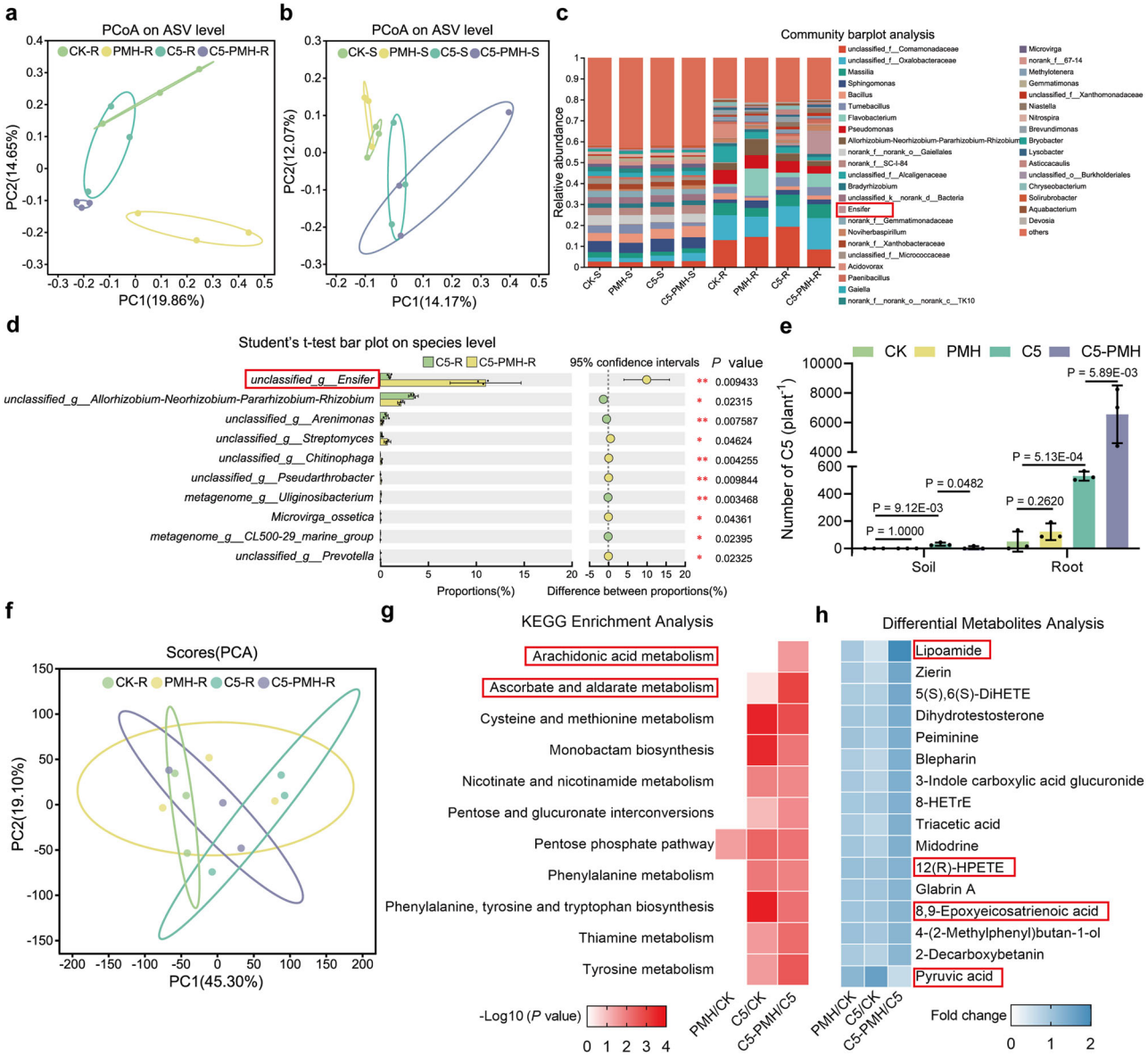

Fig. 6 | Effects of C5-loaded PMH on microbial diversity and metabolome. a, **b** Principal co-ordinates analysis (PCoA) of 16S rRNA sequencing of *Brassica napus* root (R) (**a**) and rhizosphere soil (S) (**b**) samples treated with the control group (CK), polymeric hydrogel (PMH), plant growth-promoting rhizobacteria C5, and C5-loaded PMH (C5-PMH) at the Amplicon Sequence Variant (ASV) level. **c** Community barplot analysis of 16S rRNA sequencing of *Brassica napus* root and rhizosphere soil samples at the genus level. **d** Student's *t*-test bar plot of 16S rRNA sequencing of *Brassica napus* root samples from C5 and C5-PMH groups on the species level. **e** Bar diagram of 16S rRNA sequencing of *Brassica napus* root and rhizosphere soil samples on the ASV level. **f** Principal component analysis (PCA) of *Brassica napus* root metabolites identified by LC-MS. **g** Kyoto Encyclopedia of Genes and Genomes (KEGG) pathway analysis of differentially enriched metabolites in *Brassica napus* roots. Fisher's two-tailed test is first conducted, followed by the use of the BH method for multiple testing correction. **h** Heatmaps of differential metabolites in *Brassica napus* roots. Biological repetitions are all three ($n = 3$). The error bars in (**d**, **e**) are the SD of 3 plants per biological repeat ($n = 3$). Statistically significant differences between the means were analyzed with two-tailed Student's *t*-test (*$p < 0.05$; **$p < 0.01$; ***$p < 0.001$; ****$p < 0.0001$) in (**d**, **e**).

https://doi.org/10.1038/s41467-025-56988-3

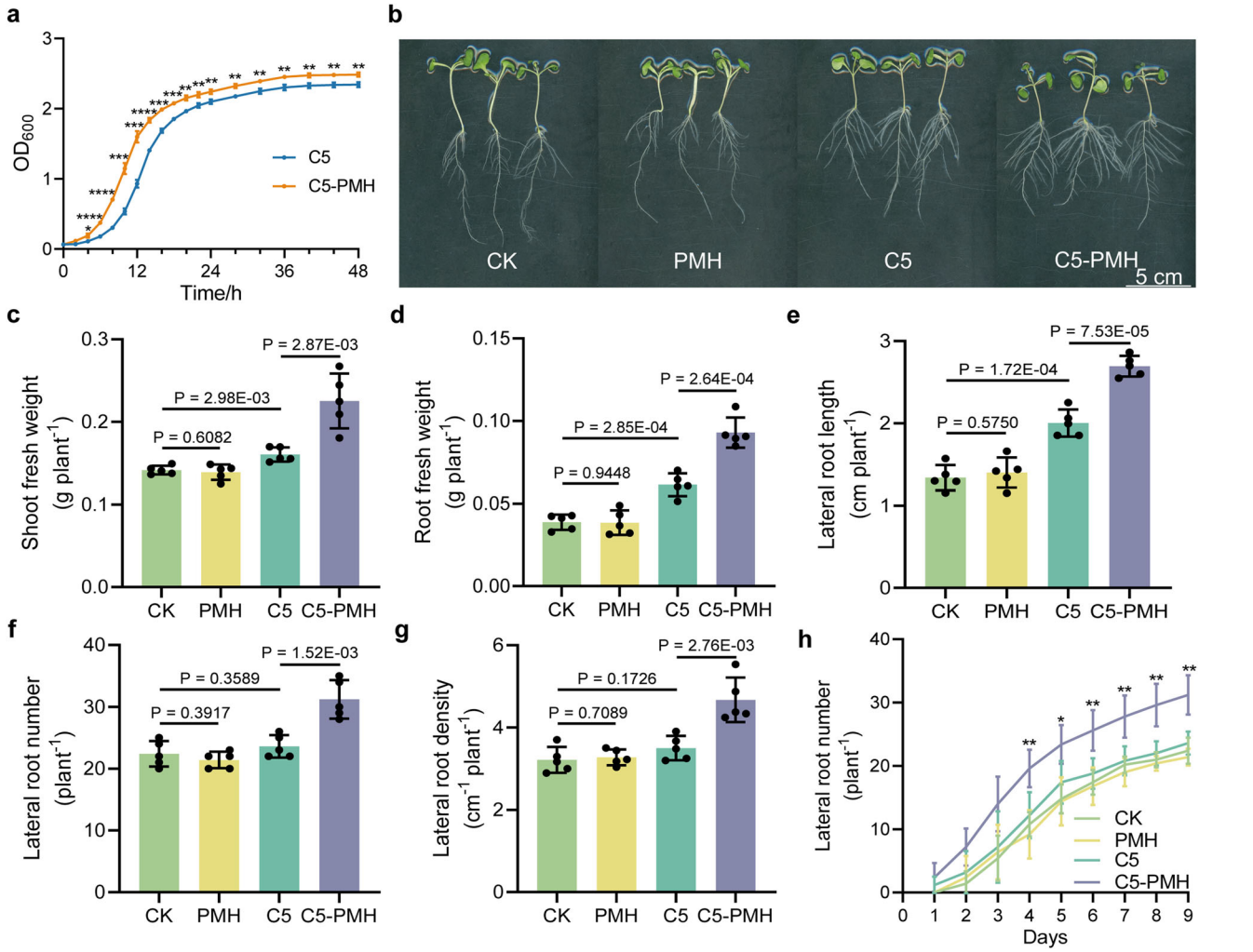

Fig. 7 | PMH preserves PGPRs and boosts their proliferation rate, thereby promoting plant growth in acidic environments (with Supplementary Figs. 7–9). **a** Growth curve of plant growth-promoting rhizobacteria C5 and C5-loaded PMH (C5-PMH) measured at OD_{600} in LB culture medium (pH = 5.5). **b** Representative images of *Brassica napus* (*Zhongshuang 11*) seedlings grown in culture medium (pH = 5.5) treated with the control group (CK), polymeric hydrogel (PMH), C5, and C5-loaded PMH (C5-PMH), scale bar = 5 cm. **c**, **d** Quantification of fresh weight of shoot (**c**) and root (**d**). **e** Growth curve on the lateral root number of *Zhongshuang 11* seedlings ("*" indicates significant difference between the C5 and C5-PMH groups, there is no significant difference between the CK, PMH, and C5 groups). **f**–**h** Quantification of lateral root length (**f**), number (**g**) and density (**h**). The error bars in (**a**) represent the SD of 3 biological replicates ($n = 3$); those in (**c**–**h**) are the SD of 5 plants per biological repeat ($n = 5$). Statistically significant differences between the means were analyzed with two-tailed Student's *t*-test (*$p < 0.05$; **$p < 0.01$; ***$p < 0.001$; ****$p < 0.0001$) in (**a**, **c**–**h**).

measured using a MCR 102 Modular Compact Rheometer (Anton Paar, Austria). In partial-component rheological measurements in PMH, the content of each component is consistent with it being in PMH. The oscillatory frequency sweep tests were carried out from 0.1 to 100 Hz at 25°C. All the measurements were repeated three times.

Feasibility analysis of wrapping PGPRs by PMH

For the culture and treatment of bacteria, LB medium was autoclaved at 121 °C for 20 min, the microorganisms were cultured in a shaker incubator at 200 rpm and 30 °C until an OD_{600} of 0.7, 11 mL of bacterial broth solution was centrifuged, supernatant was discarded to take the bacterial body, 11 mL of biopolymer solution was pipetted into the bacteria, and mixed.

The same concentration of bacterial suspension and biofertilizer were prepared and then lyophilized. After sputter-coating with gold, the morphology of the samples was examined using a Phenom Pro SEM (Phenom World, the Netherlands). The bacterial suspension and biofertilizer were separately deposited onto copper grids, air-dried, and then imaged by a HT7800 transmission electron microscopy (HITACHI, Japan).

The same concentration of bacterial solution and different wrapping agent wrapped bio-fertilizers were placed in LB medium and incubated in shaker incubator at 200 rpm and 30 °C. After a period of time, the absorbance value of the solution at 600 nm was detected to make a growth curve.

For the bacterial activity assay, standard curves were made and Alamar Blue experiments were performed according to the manufacturer's protocol (Supplementary Fig. 2)[26,63]. The samples were prepared in the dark and stored wrapped in aluminum foil prior to analysis. 100 µL of *Ensifer* C5 solution encapsulated with CMCS, SA, CMCS and SA mixtures with $CaCl_2$, and other encapsulation materials (e.g., PVP and MC) were inoculated into transparent 96-well plates and stored out of light. Bacterial activity was determined after 1, 3 and 5 weeks of storage. 10 µL of Alamar Blue was added to each well and incubated away from light. When the color of the solution started to change from indocyanine blue to pink (1.5 h), it was detected by a Varioskan LUX Multifunctional Enzyme-linked

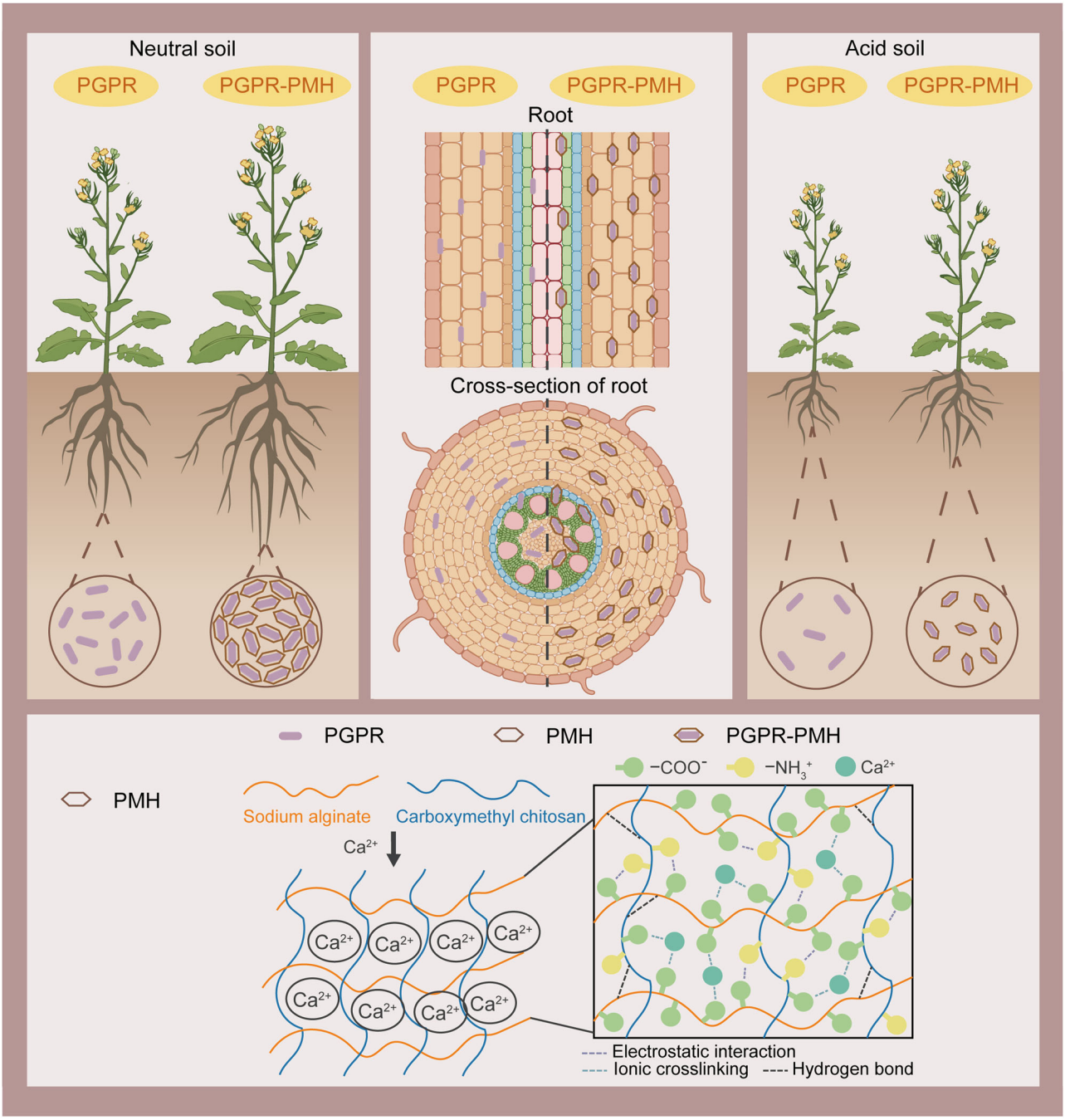

Fig. 8 | Schematic diagram of the capacity for PMH to conserve, deliver and facilitate the colonization of PGPRs for plant growth and resistance to acidic environments. Carboxymethyl chitosan (CMCS), sodium alginate (SA), and calcium chloride ($CaCl_2$) were cross-linked with each other to form biocompatible and biodegradable polymeric hydrogel (PMH). PMH can be used for encapsulation, preservation, and delivery of PGPRs, to enhance the colonization efficiency of PGPRs, produce a dosage effect to promote plant growth, and attenuate the loss of viability of PGPRs in acidic environments. Some of the elements of this figure are by figdraw.com. Created in BioRender. QR, F. (2025) https://BioRender.com/i02e296.

Immunosorbent Assay (ELISA) Reader (ThermoFisher Scientific, USA) at 530 nm excitation and at 590 nm emission. The degree of reduction of Alamar Blue is the percentage of bacterial viability.

To determine the efficacy of the CMCS/SA/Ca^{2+} polymer matrix in releasing PGPRs, we monitored the release process. Biofertilizers encapsulating GFP-C5 were placed in culture medium, and the release of bacteria from the biofertilizers into the surrounding medium was periodically imaged using an LSM780 Laser Scanning Confocal Microscope (Carl Zeiss, Germany). An increase in the number of bacteria observed in the field of view over time would confirm the effectiveness of the system.

Plant growth conditions and phenotypic analysis

Brassica napus (*Zhongshuang 11*), *Pakchoi* (*Jinzhi 30*), *Arabidopsis thaliana* Columbia-0 (Col-0), genetically modified line *DR5::GFP*[40] and mutant *gpat5*[64] were used in this study. The seeds were successively treated with 70% alcohol and 10% NaClO solution for 1 min and 10 min, rinsed with distilled water, and set aside. Soil chemical factors of sampling sites were listed in Supplementary Tables S1, S2.

For soil cultivation experiments, *B. napus* and *Pakchoi* were sown to grow in soil collected from Shilin County, Kunming, Yunnan Province (103°27′15″E, 24°75′90″N), and placed in a light incubator at 23 °C (16 h of light at 20,000 lux/8 h of darkness) for 21 days. Seedlings were treated with a combination of filtered water (CK), polymeric hydrogel (PMH), plant growth promoting rhizobacteria C5, and C5-loaded PMH (C5-PMH), respectively. On the day of sowing, 5 mL of the corresponding solution was applied to each plant. Thereafter, applications were made once a week. For the C5 and C5-PMH groups, the bacterial OD_{600} of the applied solutions was 0.7. All nutrient solutions poured are low phosphorus nutrient solutions (12.5 μmol/L). 21 days after planting, the net photosynthetic rate or SPAD value of the plants was determined with a LI-6800 Portable Photosynthesis Measurement System (LI-COR, USA) or a SPAD meter, and then the plants were dug up and rinsed with water. Leaf area was analyzed by Image J after photographing with a camera. Root length and stem diameter were measured with a soft ruler and vernier calipers, and fresh and dry weights of plant tissues were determined.

For field experiments, the field was divided into 12 plots of 1.5 m × 1.5 m each with 0.5 m row spacing, and *B. napus* were planted in a scatter design with the plots arranged in randomized complete blocks of three replications. *B. napus* grown in the greenhouse for 1 month were transplanted to the soil of Chongqing Academy of Agricultural Sciences (106°21′78″E, 29°27′57″N) with water (CK), polymeric hydrogel (PMH), plant growth promoting rhizobacteria C5, and C5- loaded PMH (C5-PMH) in a combination of treatments. On the day of transplanting, 50 mL of the corresponding solution was applied to each plant. Thereafter, applications were made once a month. For the C5 and C5-PMH groups, the bacterial OD_{600} of the applied solutions was 0.7. All applied fertilizers contain only 50% P (compared to normal). Fungicides and insecticides were sprayed to control pests and diseases, and weeds were periodically removed by hand. After 2 months, plant height and stem diameter were measured with a soft ruler and vernier calipers, and fresh and dry weights of plant tissues were determined. After maturation, the number of pods and the yield of each plant were counted.

For plate experiments, *A. thaliana* (pre-vernalized at 4 °C for 2 days) and *B. napus* were seeded into medium containing 1/2 MS (-P) and 1% agar, potassium dihydrogen phosphate was added to bring the P content to 12.5 μmol/L, and the pH of the plates was adjusted or treated with PMH, C5, or C5-loaded PMH according to experimental requirements. Plates were placed vertically in a light incubator at 22 °C (16 h of light / 8 h of darkness). Light intensity was 12,000 lux for *A. thaliana* and 20,000 lux for *B. napus*. Images of seedlings were taken at 14 days of growth. Lateral root length and lateral root density were analyzed with Image J.

Microscopic imaging of roots

Roots were imaged using an LSM780 Laser Scanning Confocal Microscope (Carl Zeiss, Germany). For bacterial colonization analysis, *B. napus* seeds were sown and grown in 1/2 MS solid medium for 5 days, seedlings were removed and roots were immersed in GFP-C5 bacterial solution or GFP-C5 bacterial fertilizer for 2 days, primary and lateral roots were cut, and lateral roots were transected with a Leica VT1000S Vibrating Microtome (Leica Corporation, Germany). Wash the roots with PBS buffer solution before imaging. Roots were carefully placed on slides, appropriate amount of PBS buffer solution was added dropwise, and coverslips were applied. The roots were then subjected to confocal microimaging[61]. For suberin staining of roots, seedlings grown for 5 days were incubated in a freshly prepared solution of Fluorol Yellow 088 (0.01% w/v, in lactic acid) for 1 h at room temperature, and then counterstained with aniline blue (0.5% w/v aqueous solution) for 30 min at room temperature in the dark. They were washed three times with water (10 min each), prepared in 50% glycerol and observed under a confocal microscope[65]. For the detection of *DR5::GFP*, roots were collected and subjected to confocal microscopy imaging.

Sample collection and DNA extraction

Fresh plant plants were collected, and after removing large pieces of soil and loose soil from the roots, residual soil was collected from the roots using sterile brushes, homogenized, and frozen at −80 °C as a sample of rhizosphere soil; plant roots were ultrasonically washed three times (50 Hz) and frozen at −80 °C as a sample for root endophyte testing[66,67].

Total root and rhizosphere soil genomic DNA was extracted from samples using a MagAtrract PowerSoil Pro DNA Kit (Qiagen, Germany) according to the manufacturer's instructions. The quality and concentration of DNA were determined by 1.0% agarose gel electrophoresis and a NanoDrop2000 spectrophotometer (Thermo Scientific, USA) and stored at −80 °C prior to further use.

16 S rRNA gene amplicon sequencing for bacterial community analysis

The hypervariable region V5-V7 of the bacterial 16 S rRNA gene was amplified using an ABI GeneAmp® 9700 PCR Thermal Cycler (Applied Biosystems, USA) with amplification primers 799 F (5′-AACMGGATTAGATACCCKG-3′) and 1193 R (5′-ACGTCATCCCCACCTTCC-3′)[68,69]. PCR conditions were as follows: initial denaturation at 95 °C for 3 min, followed by denaturation at 95 °C for 30 s, annealing at 55 °C for 30 s, extension at 72 °C for 45 s, followed by a single extension at 72 °C for 10 min, and termination at 4 °C. PCR product concentrations were measured using a QuantiFluor™ -ST blue fluorescence quantification system (Promega, USA) and all samples were standardized. Purified amplicons were pooled in equimolar form and subjected to bipartite sequencing on the Illumina MiSeq PE250 platform (Illumina, USA) according to the standard protocols of Majorbio Bio-Pharm Technology Co. Ltd (Shanghai, China). After the PE reads obtained from sequencing were sample split, the bipartite reads were quality controlled and filtered according to the sequencing quality, and at the same time spliced according to the overlap relationship between the bipartite Reads, to obtain the optimized data after quality controlled splicing. DADA2 is used for quality filtering (i.e., filtering, de-duplication, de-noising, merging, and evaluating chimeras) of raw 16S rRNA gene amplicon sequencing reads through QIIME2[70]. Amplicon Sequence Variant (ASV) identified as chloroplasts or mitochondria was removed. Next, the feature table generated by DADA2 is filtered to remove ASVs with frequencies <2 to obtain ASV representative sequences and abundance information[71]. Principal co-ordinates analysis (PCoA) and Bray-Curtis distance calculations were performed by R (version 3.3.1) based on relative abundance of ASVs. Community Bar maps were analyzed by python-2.7. Species difference analysis was done based on Student's *t*-test. The C5 sequences were compared with the representative sequences of ASVs, and the ASVs with the highest similarity were selected for C5 enrichment analysis.

Root metabolite analysis

Metabolites were extracted from plant root samples using methanol:water = 4:1 (v/v) solution, the mixture was crushed, sonicated and centrifuged, and the supernatant was transferred to sample bottles for machine analysis[72]. Quality control (QC) samples were prepared by mixing equal volumes of all sample metabolites to examine the reproducibility of the entire analytical process[73]. The samples were analyzed by LC-MS on a UHPLC-Q Exactive HF-X system (Thermo Fisher Scientific, USA) equipped with an ACQUITY HSS T3 column (100 mm × 2.1 mm i.d., 1.8 μm; Waters, USA). After analysis, LC-MS raw data were imported into the metabolomics processing software Progenesis QI (Waters Corporation, USA) for peak detection and alignment. Data analysis was performed on an online analysis platform (Majorbio Biotech Co., Ltd., Shanghai, China). The identified metabolites were annotated to the KEGG database (https://www.kegg.jp/).

Reverse transcription-polymerase chain reaction (RT-PCR)

B. napus (*Zhongshuang 11*) seedlings were cultivated in in soil for 21 days. The root samples were harvested to extract RNA using EZ-10 DNAaway RNA Mini-Preps kit (Product Number: B618133-0250, Sangon Biotech, China). Reverse transcription was performed with Biometra TOne 96 G Gradient PCR Thermal Cycler (Jena Analytical Instruments GmbH, Germany) and PrimeScript™ RT reagent Kit with gDNA Eraser (Perfect Real Time) (Code No. RR047A, Takara, Japan). PCR was performed on QuantStudio 1 Real-time quantitative PCR system (Thermo Fisher Scientific, USA). Actin7 was used as an internal reference. The primers for RT-PCR were listed in Supplementary Table S3 (Tsingke Biotech, China).

Reporting summary

Further information on research design is available in the Nature Portfolio Reporting Summary linked to this article.

Data availability

The 16S rRNA data from this study have been submitted to NCBI and and can be accessed through BioProject PRJNA1212299: http://www.ncbi.nlm.nih.gov/bioproject/1212299. The metabolomics data have been uploaded to Figshare and can be accessed via https://doi.org/10.6084/m9.figshare.28233716. Genome information for C5 been uploaded to Figshare and can be accessed via https://doi.org/10.6084/m9.figshare.28233677. Source data is available for Figs. 1–7 and Supplementary Figs. 1–9 in the associated source data file. Source data are provided with this paper.

References

1. Kah, M., Tufenkji, N. & White, J. C. Nano-enabled strategies to enhance crop nutrition and protection. *Nat. Nanotechnol.* **14**, 532–540 (2019).
2. Carvajal-Yepes, M. et al. A global surveillance system for crop diseases. *Science* **364**, 1237–1239 (2019).
3. van Vliet, J., Eitelberg, D. A. & Verburg, P. H. A global analysis of land take in cropland areas and production displacement from urbanization. *Glob. Environ. Change Hum. Policy Dimens.* **43**, 107–115 (2017).
4. Borrelli, P. et al. Land use and climate change impacts on global soil erosion by water (2015–2070). *Proc. Natl. Acad. Sci. USA* **117**, 21994–22001 (2020).
5. Tang, F. H., Lenzen, M., McBratney, A. & Maggi, F. Risk of pesticide pollution at the global scale. *Nat. Geosci.* **14**, 206–210 (2021).
6. McElwee, P. et al. The impact of interventions in the global land and agri-food sectors on nature's contributions to people and the UN sustainable development goals. *Glob. Change Biol.* **26**, 4691–4721 (2020).
7. Hofmann, T. et al. Technology readiness and overcoming barriers to sustainably implement nanotechnology-enabled plant agriculture. *Nat. Food* **1**, 416–425 (2020).
8. Waigi, M. G., Sun, K. & Gao, Y. Sphingomonads in microbe-assisted phytoremediation: tackling soil pollution. *Trends Biotechnol.* **35**, 883–899 (2017).
9. Perreault, R. & Laforest-Lapointe, I. Plant-microbe interactions in the phyllosphere: facing challenges of the anthropocene. *ISME J.* **16**, 339–345 (2022).
10. Jansson, J. K., McClure, R. & Egbert, R. G. Soil microbiome engineering for sustainability in a changing environment. *Nat. Biotechnol.* **41**, 1716–1728 (2023).
11. Wang, N. Q. et al. Microbiome convergence enables siderophore-secreting-rhizobacteria to improve iron nutrition and yield of peanut intercropped with maize. *Nat. Commun.* **15**, 17 (2024).
12. Arif, I., Batool, M. & Schenk, P. M. Plant microbiome engineering: expected benefits for improved crop growth and resilience. *Trends Biotechnol.* **38**, 1385–1396 (2020).
13. Song, S. Y. et al. PSKR1 balances the plant growth-defence trade-off in the rhizosphere microbiome. *Nat. Plants* **9**, 2071–2084 (2023).
14. Raza, W. et al. Microbe-induced phenotypic variation leads to overyielding in clonal plant populations. *Nat. Ecol. Evol.* **8**, 392–399 (2024).
15. Britt, D. W. Plug-and-play bioinspired seed coatings. *Nat. Food* **2**, 456–457 (2021).
16. Riseh, R. S., Hassanisaadi, M., Vatankhah, M. & Kennedy, J. F. Encapsulating biocontrol bacteria with starch as a safe and edible biopolymer to alleviate plant diseases: a review. *Carbohyd. Polym.* **302**, 120384 (2023).
17. Zvinavashe, A. T., Mardad, I., Mhada, M., Kouisni, L. & Marelli, B. Engineering the plant microenvironment to facilitate plant-growth-promoting microbe association. *J. Agric. Food Chem.* **69**, 13270–13285 (2021).
18. Li, M. S. et al. Nano-enabled strategies to enhance biological nitrogen fixation. *Nat. Nanotechnol.* **18**, 688–691 (2023).
19. Ahmed, T., Noman, M., Gardea-Torresdey, J. L., White, J. C. & Li, B. Dynamic interplay between nano-enabled agrochemicals and the plant-associated microbiome. *Trends Plant Sci.* **28**, 1310–1325 (2023).
20. Zhang, M.-X. et al. Potential roles of iron nanomaterials in enhancing growth and nitrogen fixation and modulating rhizomicrobiome in alfalfa (Medicago sativa L.). *Bioresour. Technol.* **391**, 129987 (2024).
21. Cao, Y., Lim, E., Xu, M., Weng, J. K. & Marelli, B. Precision delivery of multiscale payloads to tissue-specific targets in plants. *Adv. Sci.* **7**, 1903551 (2020).
22. Zhang, Y., Huang, C. & Xiong, R. Advanced materials for intracellular delivery of plant cells: Strategies, mechanisms and applications. *Mater. Sci. Eng. R. Re.* **160**, 100821 (2024).
23. Croissant, J. G., Butler, K. S., Zink, J. I. & Brinker, C. J. Synthetic amorphous silica nanoparticles: toxicity, biomedical and environmental implications. *Nat. Rev. Mater.* **5**, 886–909 (2020).
24. Nair, L. S. & Laurencin, C. T. Biodegradable polymers as biomaterials. *Prog. Polymer Sci.* **32**, 762–798 (2007).
25. Zvinavashe, A. T. et al. Programmable design of seed coating function induces water-stress tolerance in semi-arid regions. *Nat. Food* **2**, 485–493 (2021).
26. Zvinavashe, A. T., Lim, E., Sun, H. & Marelli, B. A bioinspired approach to engineer seed microenvironment to boost germination and mitigate soil salinity. *Proc. Natl. Acad. Sci. USA.* **116**, 25555–25561 (2019).
27. Chouhan, G. K. et al. Phytomicrobiome for promoting sustainable agriculture and food security: opportunities, challenges, and solutions. *Microbiol. Res.* **248**, 126763 (2021).
28. Singh, B. K., Trivedi, P., Egidi, E., Macdonald, C. A. & Delgado-Baquerizo, M. Crop microbiome and sustainable agriculture. *Nat. Rev. Microbiol.* **18**, 601–602 (2020).
29. O'Callaghan, M. Microbial inoculation of seed for improved crop performance: issues and opportunities. *Appl. Microbiol. Biotechnol.* **100**, 5729–5746 (2016).
30. Compant, S., Samad, A., Faist, H. & Sessitsch, A. A review on the plant microbiome: ecology, functions, and emerging trends in microbial application. *J. Adv. Res.* **19**, 29–37 (2019).
31. Wang, H. et al. A sodium alginate/carboxymethyl chitosan dual-crosslinked injectable hydrogel scaffold with tunable softness/hardness for bone regeneration. *Int. J. Biol. Macromol.* **257**, 128700 (2024).
32. Sun, J.-Y. et al. Highly stretchable and tough hydrogels. *Nature* **489**, 133–136 (2012).
33. Tang, S. et al. Construction of physically crosslinked chitosan/sodium alginate/calcium ion double-network hydrogel and its application to heavy metal ions removal. *Chem. Eng. J.* **393**, 124728 (2020).

34. Peng, K. et al. Preparation of chitosan/sodium alginate conductive hydrogels with high salt contents and their application in flexible supercapacitors. *Carbohyd. Polym.* **278**, 118927 (2022).
35. He, Y. et al. A double-network polysaccharide-based composite hydrogel for skin wound healing. *Carbohyd. Polym.* **261**, 117870 (2021).
36. Wang, R. et al. Poly-γ-glutamic acid microgel-encapsulated probiotics with gastric acid resistance and smart inflammatory factor targeted delivery performance to ameliorate colitis. *Adv. Funct. Mater.* **32**, 2113034 (2022).
37. Paz-Ares, J. et al. Plant adaptation to low phosphorus availability: core signaling, crosstalks, and applied implications. *Mol. Plant.* **15**, 104–124 (2022).
38. Yang, S. Y., Lin, W. Y., Hsiao, Y. M. & Chiou, T. J. Milestones in understanding transport, sensing, and signaling of the plant nutrient phosphorus. *Plant Cell* **36**, 1504–1523 (2024).
39. Salas-González, I. et al. Coordination between microbiota and root endodermis supports plant mineral nutrient homeostasis. *Science* **371**, eabd0695 (2021).
40. Blilou, I. et al. The PIN auxin efflux facilitator network controls growth and patterning in Arabidopsis roots. *Nature* **433**, 39–44 (2005).
41. Savchenko, T. et al. Arachidonic acid: an evolutionarily conserved signaling molecule modulates plant stress signaling networks. *Plant Cell* **22**, 3193–3205 (2010).
42. Złotek, U., Szymanowska, U., Jakubczyk, A., Sikora, M. & Świeca, M. Effect of arachidonic and jasmonic acid elicitation on the content of phenolic compounds and antioxidant and anti-inflammatory properties of wheatgrass (Triticum aestivum L.). *Food Chem.* **288**, 256–261 (2019).
43. Zhao, L. et al. Metabolomics reveals the molecular mechanisms of copper induced cucumber leaf (Cucumis sativus) senescence. *Environ. Sci. Technol.* **52**, 7092–7100 (2018).
44. Bai, C. et al. Multiomics analyses of the effects of LED white light on the ripening of apricot fruits. *J. Adv. Res.* **67**, 1–13 (2025).
45. Mathias, R. A. et al. Sirtuin 4 is a lipoamidase regulating pyruvate dehydrogenase complex activity. *Cell* **159**, 1615–1625 (2014).
46. Škerlová, J., Berndtsson, J., Nolte, H., Ott, M. & Stenmark, P. Structure of the native pyruvate dehydrogenase complex reveals the mechanism of substrate insertion. *Nat. Commun.* **12**, 5277 (2021).
47. Mattevi, A. How evolution dismantles and reassembles multienzyme complexes. *Proc. Natl Acad. Sci. USA* **119**, e2120286118 (2022).
48. Timm, S. et al. Mitochondrial dihydrolipoyl dehydrogenase activity shapes photosynthesis and photorespiration of Arabidopsis thaliana. *Plant Cell* **27**, 1968–1984 (2015).
49. Jing, H. J. et al. Facile synthesis of pH-responsive sodium alginate/carboxymethyl chitosan hydrogel beads promoted by hydrogen bond. *Carbohyd. Polym.* **278**, 10 (2022).
50. Ahmed, T. et al. Green molybdenum nanoparticles-mediated biostimulation of Bacillus sp. strain ZH16 improved the wheat growth by managing in planta nutrients supply, ionic homeostasis and arsenic accumulation. *J. Hazard. Mater.* **423**, 11 (2022).
51. Zhang, H. et al. Natural phenolic-metal framework strengthened mesona chinensis polysaccharides microgels for improved viability of probiotics to alleviate the liver injury and gut microbiota dysbiosis. *Adv. Funct. Mater.* **34**, 2401064 (2024).
52. Haro-González, J. N., de Alba, B. N. S., Morales-Hernández, N. & Espinosa-Andrews, H. Type A gelatin-amidated low methoxyl pectin complex coacervates for probiotics protection: formation, characterization, and viability. *Food Chem.* **453**, 139644 (2024).
53. Gu, S. et al. Intracellularly gelated macrophages loaded with probiotics for therapy of colitis. *Nano Lett.* **24**, 13504–13512 (2024).
54. Wang, X. et al. The growth-promoting mechanism of Brevibacillus laterosporus AMCC100017 on apple rootstock Malus robusta. *Horticultural Plant J.* **8**, 22–34 (2022).
55. Panichikkal, J., Prathap, G., Nair, R. A. & Krishnankutty, R. E. Evaluation of plant probiotic performance of Pseudomonas sp. encapsulated in alginate supplemented with salicylic acid and zinc oxide nanoparticles. *Int. J. Biol. Macromol.* **166**, 138–143 (2021).
56. Szopa, D. et al. Encapsulation efficiency and survival of plant growth-promoting microorganisms in an alginate-based matrix–A systematic review and protocol for a practical approach. *Ind. Crops Prod.* **181**, 114846 (2022).
57. Kochian, L. V., Piñeros, M. A., Liu, J. & Magalhaes, J. V. Plant adaptation to acid soils: the molecular basis for crop aluminum resistance. *Ann. Rev. Plant Biol.* **66**, 571–598 (2015).
58. Zhou, J. et al. Programmable probiotics modulate inflammation and gut microbiota for inflammatory bowel disease treatment after effective oral delivery. *Nat. Commun.* **13**, 3432 (2022).
59. Anselmo, A. C., McHugh, K. J., Webster, J., Langer, R. & Jaklenec, A. Layer-by-layer encapsulation of probiotics for delivery to the microbiome. *Adv. Mater.* **28**, 9486 (2016).
60. El-Shetehy, M. et al. Silica nanoparticles enhance disease resistance in Arabidopsis plants. *Nat. Nanotechnol.* **16**, 344–353 (2021).
61. Sun, X. D. et al. Magnetite nanoparticle coating chemistry regulates root uptake pathways and iron chlorosis in plants. *Proc. Natl. Acad. Sci. USA* **120**, 8 (2023).
62. Lukashuk, L. et al. Operando insights into CO oxidation on cobalt oxide catalysts by NAP-XPS, FTIR, and XRD. *ACS Catal.* **8**, 8630–8641 (2018).
63. Gliga, A. R., Skoglund, S., Odnevall Wallinder, I., Fadeel, B. & Karlsson, H. L. Size-dependent cytotoxicity of silver nanoparticles in human lung cells: the role of cellular uptake, agglomeration and Ag release. *Particle Fibre Toxicol.* **11**, 1–17 (2014).
64. Beisson, F., Li, Y., Bonaventure, G., Pollard, M. & Ohlrogge, J. B. The acyltransferase GPAT5 is required for the synthesis of suberin in seed coat and root of Arabidopsis. *Plant Cell* **19**, 351–368 (2007).
65. Ursache, R. et al. GDSL-domain proteins have key roles in suberin polymerization and degradation. *Nat. Plants* **7**, 353–364 (2021).
66. Edwards, J. et al. Structure, variation, and assembly of the root-associated microbiomes of rice. *Proc. Natl. Acad. Sci. USA* **112**, E911–E920 (2015).
67. Panke-Buisse, K., Poole, A. C., Goodrich, J. K., Ley, R. E. & Kao-Kniffin, J. Selection on soil microbiomes reveals reproducible impacts on plant function. *ISME J.* **9**, 980–989 (2015).
68. Bulgarelli, D. et al. Revealing structure and assembly cues for Arabidopsis root-inhabiting bacterial microbiota. *Nature* **488**, 91–95 (2012).
69. Bulgarelli, D. et al. Structure and function of the bacterial root microbiota in wild and domesticated barley. *Cell Host Microbe.* **17**, 392–403 (2015).
70. Bolyen, E. et al. Reproducible, interactive, scalable and extensible microbiome data science using QIIME 2. *Nat. Biotechnol.* **37**, 852–857 (2019).
71. Callahan, B. J. et al. DADA2: High-resolution sample inference from Illumina amplicon data. *Nat. Methods* **13**, 581–583 (2016).
72. Kong, X. et al. Acetic acid alters rhizosphere microbes and metabolic composition to improve willows drought resistance. *Sci. Total Environ.* **844**, 157132 (2022).
73. Zhao, M. et al. Microplastics promoted cadmium accumulation in maize plants by improving active cadmium and amino acid synthesis. *J. Hazard. Mater.* **447**, 13 (2023).

Acknowledgements

This work was supported by the National Key R & D Program of China (2022YFD1900705), National Natural Foundation of China (32072102, 31671728), Youth Top Talent Project, the SWU Youth Leadership Team

Project (SWU-XJLJ202308), and the Shuangcheng Cooperative Agreement Research Grant of Yibin, China (XNDX2022020003) for N.Li, Key Research Project Plan of Higher Education Institutions in Henan Province(22A210001) for Y.Wang.

Author contributions

Q.F., Y.L., Y.C., B.X., and N.L. designed research; Q.F., Y.L., M.L., Y.C., L.W. performed research; C.L., X.Z., L.R., Y.W., D.W., Y.T.Z., and Y.F.Z. contributed materials and tools; Q.F. analyzed data; and Q.F., B.X., and N.L. wrote the paper.

Competing interests

The authors declare no competing interests.

Additional information

Supplementary information The online version contains supplementary material available at https://doi.org/10.1038/s41467-025-56988-3.

Correspondence and requests for materials should be addressed to Bo Xiao or Nannan Li.

Peer review information *Nature Communications* thanks Wenling Yang, and the other, anonymous, reviewers for their contribution to the peer review of this work. A peer review file is available.